ACS chemical biology

Articles

pubs.acs.org/acschemicalbiology

A Fluorescent Hsp90 Probe Demonstrates the Unique Association between Extracellular Hsp90 and Malignancy *in Vivo*

Lauren B. Crowe,[†,▽] Philip F. Hughes,[‡,▽] David A. Alcorta,[§] Takuya Osada,[∥] Aaron P. Smith,[‡] Juliane Totzke,[‡] David R. Loiselle,[‡] Isaac D. Lutz,[‡] Madhusudhana Gargesha,[⊥] Debasish Roy,[⊥] Jose Roques,[#] David Darr,[#] H. Kim Lyerly,[∥] Neil L. Spector,[‡] and Timothy A.J. Haystead*[,‡]

[†]Department of Cell Biology, Duke University, Durham, North Carolina 27710, United States

[‡]Department of Pharmacology and Cancer Biology, Duke University, Durham, North Carolina 27710, United States

[§]Department of Medicine, Duke University, Durham, North Carolina 27710, United States

[∥]Department of Surgery, Duke University, Durham, North Carolina 27710, United States

[⊥]BioInVision, Inc., Mayfield Village, Ohio 44143, United States

[#]Lineberger Comprehensive Cancer Center, University of North Carolina, Chapel Hill, North Carolina 27599, United States

Supporting Information

ABSTRACT: Extracellular expression of heat shock protein 90 (eHsp90) by tumor cells is correlated with malignancy. Development of small molecule probes that can detect eHsp90 *in vivo* may therefore have utility in the early detection of malignancy. We synthesized a cell impermeable far-red fluorophore-tagged Hsp90 inhibitor to target eHsp90 *in vivo*. High resolution confocal and lattice light sheet microscopy show that probe-bound eHsp90 accumulates in punctate structures on the plasma membrane of breast tumor cells and is actively internalized. The extent of internalization correlates with tumor cell aggressiveness, and this process can be induced in benign cells by overexpressing p110HER2. Whole body cryoslicing, imaging, and histology of flank and spontaneous tumor-bearing mice strongly suggests that eHsp90 expression and internalization is a phenomenon unique to tumor cells *in vivo* and may provide an "Achilles heel" for the early diagnosis of metastatic disease and targeted drug delivery.

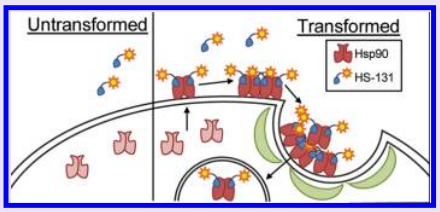

Heat shock protein 90 (Hsp90) comprises 1−3% of the cellular protein and acts as a molecular chaperone for over 200 client proteins.[1,2] Many cancer cells upregulate Hsp90 expression and are believed to be "addicted" to the protein to maintain proper folding of overexpressed oncoproteins.[3] Thus, 17 distinct Hsp90 inhibitors have entered clinical trials as potential cancer treatments.[4] These inhibitors bind to the ATP-binding pocket of Hsp90 and its paralogs GRP94 and TRAP1, inhibiting chaperone function.[5] In tumor cells, inhibiting Hsp90 results in the degradation of oncogenic client proteins and arrest of cell growth. When administered as a monotherapy in clinical studies, Hsp90 inhibitors tend to promote tumor growth arrest rather than regression,[4] which is generally thought to be related to a compensatory induction of Hsp70. However, if drug surveillance is maintained, responsive patients remain in stable disease.[6]

The great conundrum of Hsp90 therapy is the molecular mechanism by which Hsp90 inhibitors exhibit any therapeutic efficacy given its abundance and ubiquitous expression *in vivo*. Genetic deletion studies have shown that Hsp90 is essential for normal cell function;[3] yet, systemic inhibition of Hsp90 is well tolerated in humans, with dose-limiting toxicities characterized by diarrhea and a reversible night blindness with some Hsp90 inhibitors.[7] The biodistribution of radio-labeled PUH71, a cell permeable Hsp90 inhibitor, has been studied in mice bearing MDA-MB-468 xenografts.[8,9] Consistent with the broad expression of Hsp90, radioactivity was initially detected in all tissues. However, 24 h after injection, the tumor became visible due to clearance of the drug from normal tissues and drug retention in the tumor. An earlier study hypothesized that Hsp90 in cancer cells is in a more active conformation by existing in a complex with several cochaperones. Hsp90 in this "active" conformation has a higher affinity for ATP and Hsp90 inhibitors and is thus more susceptible to inhibition.[10] In addition, Hsp90 phosphorylation by the mitotic checkpoint kinase Mps1 results in increased Hsp90 client association and sensitivity to cell-permeable Hsp90 inhibitors, such as SNX2112 and Ganetespib, in renal cancer cells.[11−13]

Of interest to us is an extracellular Hsp90 (eHsp90) and its association with malignant behavior.[14,15] In tumor cells, eHsp90 is thought to chaperone external proteins responsible for migration and metastasis, such as matrix metalloproteinases. Previous work by our group with fluorophore-tethered Hsp90 inhibitors also confirmed trafficking of Hsp90 to the cell surface but also showed that the protein was reinternalized.[16] Two groups have also demonstrated reinternalization of eHsp90 in dendritic antigen presenting cells and hypothesize that it is required for antigen cross presentation, and its reinternalization is a dynamin-independent Cdc42-dependent process.[12,17]

Received: January 3, 2017
Accepted: January 19, 2017
Published: January 19, 2017

DOI: 10.1021/acschembio.7b00006
ACS Chem. Biol. 2017, 12, 1047−1055

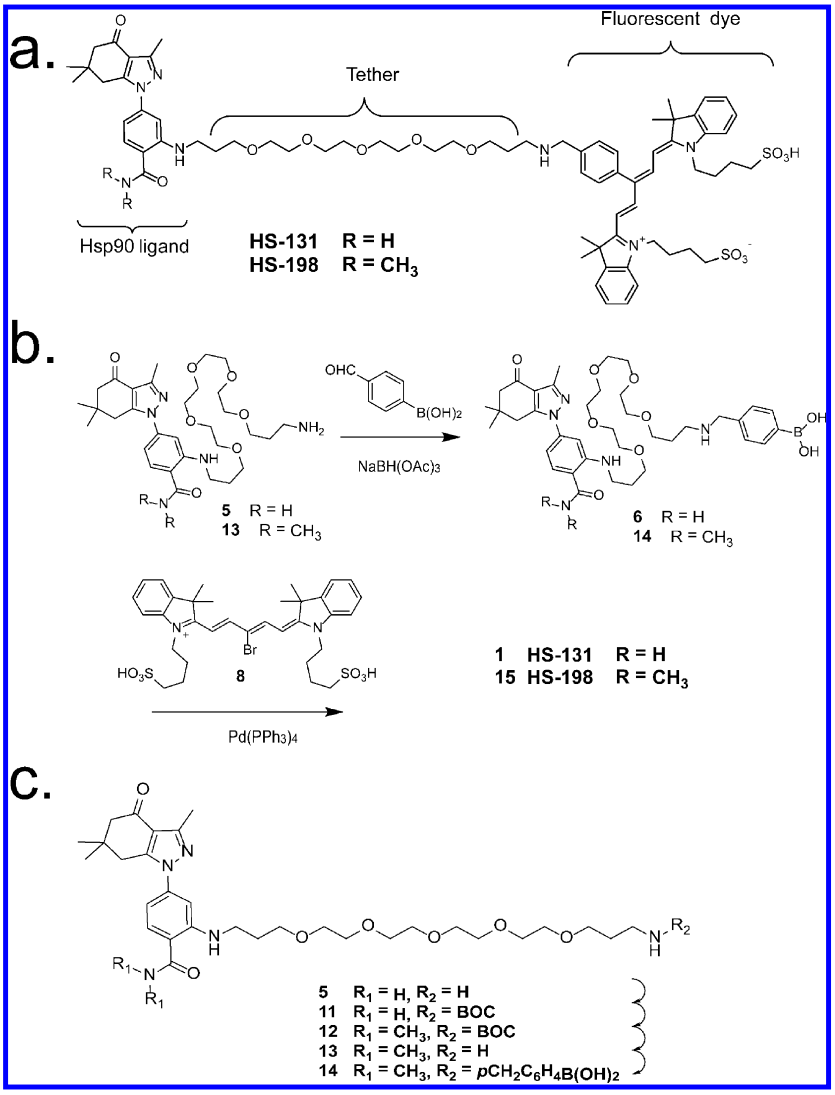

Figure 1. HS-131 and HS-198 synthesis. (a) Structure of far-red fluorescent probes, HS-131 and HS-198. (b) Synthesis scheme of HS-131 and HS-198. (c) Simplified synthesis scheme of HS-198 precursor **14**. See also Figure S2.

Together, these studies suggest that expression of eHsp90 and reinternalization has specific functions *in vivo*.

To explore eHsp90 expression *in vivo*, we developed the eHsp90 inhibitor HS-131 and its inactive analog HS-198. We show that these far-red dye-tethered Hsp90 inhibitors can be reproducibly synthesized and fluoresce at wavelengths that have low natural background fluorescence. Microscopic analysis shows that probe binding promotes eHsp90 aggregation followed by internalization in more aggressive tumor cells. Furthermore, overexpression of oncogenic p110HER2 in benign cells stimulates eHsp90 trafficking, aggregation, and reinternalization, suggesting that cycling of the protein is part of a larger oncogenic process associated with malignancy. Finally, full microscopic analysis of mice bearing either flank or spontaneous mammary tumors underscores the uniqueness of eHsp90 expression and internalization in tumor cells.

RESULTS AND DISCUSSION

Synthesis and Characterization of HS-131. Previously, we reported on the synthesis and characterization of tethered Hsp90 inhibitors, HS-69 and HS-27, consisting of a modified Hsp90 inhibitor tethered to a near-infrared (nIR) probe and FITC, respectively.[16] However, HS-27 was not optimized for higher resolution confocal imaging or tissue penetration, and HS-69 was tethered to an expensive and proprietary nIR dye of partially unknown structure *via* a potentially labile amide linker. We thus decided to synthesize a new Hsp90 inhibitor, HS-131, tethered to a Cy5 dye that was more stable and reproducibly synthesized (Figure 1a). A far-red probe with peak wavelengths of excitation and emission at 646 and 665 nm, respectively (Figure S1a), was chosen over a nIR dye to maintain imaging compatibility. On HS-198, a critical primary amide required for inhibitor binding in the active site of Hsp90 is replaced with a dimethyl amide group that precludes the formation of a critical hydrogen bond within the ATP-binding pocket of Hsp90.[18]

The complete synthesis of HS-131 and HS-198 is shown in Figure 1b. The tethered Hsp90 ligand **5**, HS-23,[19] was converted by reductive amination to the boronic acid **6**. An amine linkage was chosen to avoid hydrolytic liabilities *in vivo*. Suzuki coupling[20] with dye **8**[21] produced HS-131. HS-198 was prepared

DOI: 10.1021/acschembio.7b00006
ACS Chem. Biol. 2017, 12, 1047−1055

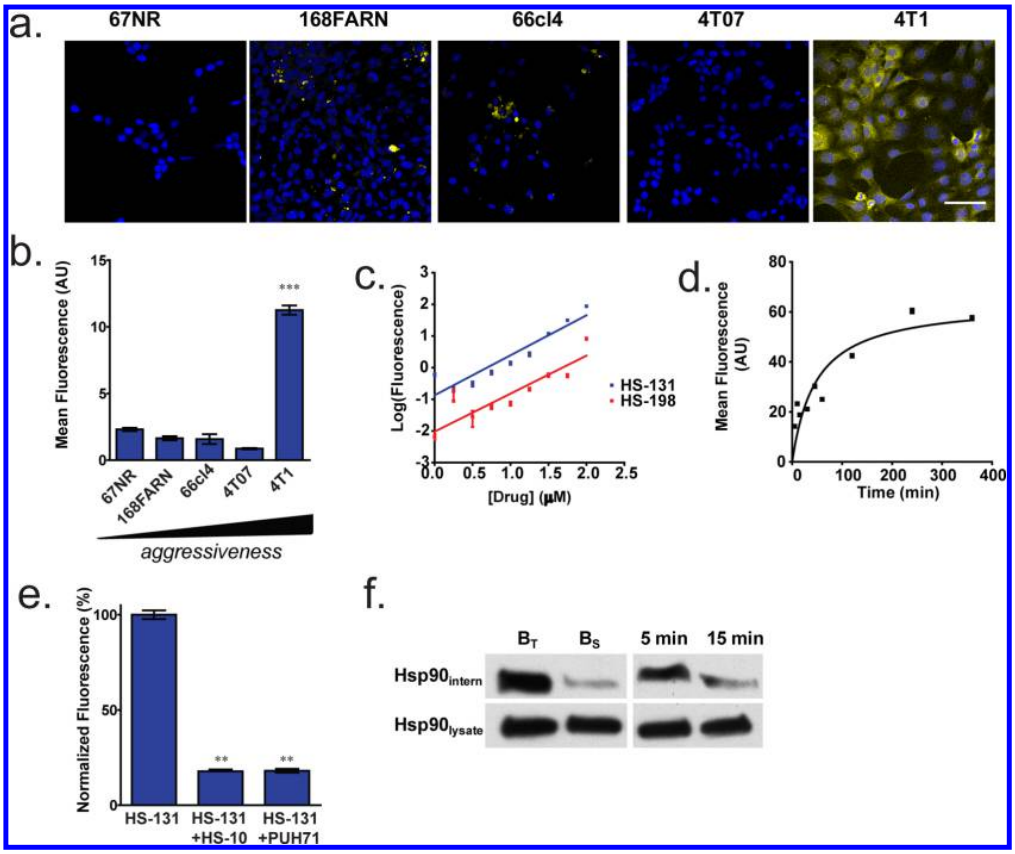

Figure 2. HS-131, a fluorescent specific small-molecule Hsp90 inhibitor. (a) Internalization of HS-131 (25 μM, 45 min) in 67NR, 168FARN, 66cl4, 4T07, and 4T1 cells, quantified in b; scale bar = 50 μm. (c) Dose-dependent internalization of HS-131 and HS-198 in MDA-MB-468 cells. (d) HS-131 is internalized in a time-dependent manner. (e) Fluorescence of HS-131-treated MDA-MB-468 cells (25 μM, 45 min) in competition with 1 μM HS-10 or 10 μM PUH71. (f) Biotinylated eHsp90 is detected *via* Western blot. B_T, total biotinylated lysate, and B_S, biotinylated lysate from stripped cells. Cells were incubated at 37 °C to stimulate endocytosis, cooled, and stripped of external biotin. $^{**}p < 0.001$, $^{***}p < 0.0001$; univariate ANOVA with Bonferroni's posthoc test. Data are represented as the means ± SEM. See also Figure S1.

in analogous fashion from amine **13**. Amine **13** was prepared from amine **5** as shown in Figure 1c. Amine **5** was first protected as the BOC amide **11**. The primary amide was then alkylated by treating **11** with sodium t-butoxide in THF followed by slow addition of methyl iodide. Chromatography gave the clean dimethyl amide **12** with 45% yield. Analysis of the ^{1}H NMR and COSY spectra of **12** showed the addition of two methyl groups, loss of the primary amide protons, and retention of the aniline and BOC amide protons. Deprotection with TFA afforded the desired amine **13**, which was converted as described above to HS-198 (Figure 1c). Complete synthesis details are listed in the Supporting Information Methods.

In a thermal stability assay,[16,19] HS-131 but not HS-198 stabilized purified Hsp90 (Figure S1b,c). In addition, HS-23, which mimics the structure of HS-131 without the fluorophore, showed specificity to Hsp90 over Grp94 at higher concentrations, unlike previously published inhibitor HS-10 (Figure S1d). Furthermore, HS-131 specifically eluted Hsp90 from lysates applied to an ATP resin, whereas HS-10 and Ganetespib eluted Hsp90 and Grp94 (Figure S1e). HS-198 did not elute Hsp90 except at high concentrations. None of the tested drugs eluted TRAP1 from the ATP resin. Studies with HS-152 (Figure S2b), containing the Cy5 fluorophore and PEG linker but lacking the Hsp90 ligand, showed no affinity for Hsp90 in thermal stability or in ATP competition studies, ruling out any contribution of the fluorophore moiety to protein binding (Figures S1b,c, S3a-c). These studies support the specificity of HS-131 for Hsp90.

HS-131 Visualizes Tumor Cell-Specific eHsp90. HS-131 is not cell permeable and binds exclusively to eHsp90, allowing us specific access to this particular pool of one of the most abundant proteins in the cell. To analyze the internalization of eHsp90 in transformed cells, we utilized the 4T1 cell model. The five isogenic cell lines (67NR, 168FARN, 66cl4, 4T07, and 4T1) are isolated from a single spontaneous mammary tumor and exhibit varying degrees of metastatic disease when injected into mice.[22] HS-131 was internalized more in 4T1 cells (the most aggressive of the five lines) over the less metastatic lines (Figures 2a,b). In MDA-MB-468 cells, uptake of HS-131 was dose- and time-dependent (Figure 2c,d), and binding of the probe to eHsp90 was competed with HS-10 and PUH71 (Figure 2e). In contrast, the inactive analog HS-198 was only weakly internalized at higher concentrations (Figure 2c).

Hsp90 Internalization Is Inhibitor-Independent. To determine if eHsp90 internalization is dependent on Hsp90 inhibition by HS-131 or is a natural oncogenic mechanism, we employed a biotin internalization assay.[23] Cells were treated on ice with amine-reactive biotin to label extracellular proteins. The cells were returned to 37 °C to allow for endocytosis, cooled again, and stripped of any extracellular biotin. By Western blot of

DOI: 10.1021/acschembio.7b00006
ACS Chem. Biol. 2017, 12, 1047−1055

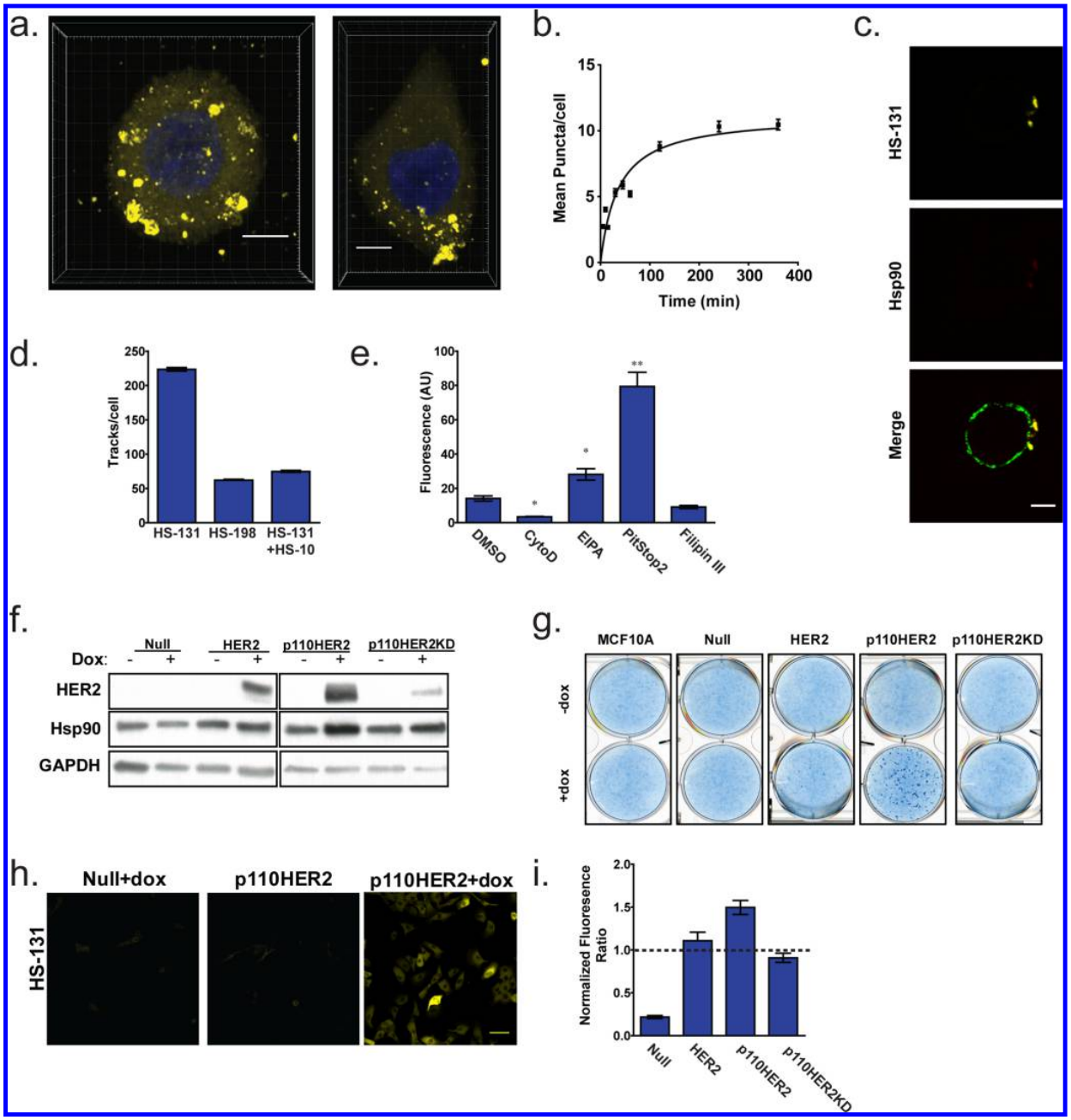

Figure 3. HS-131 accumulating into Hsp90-positive puncta within the cell and induced by transformation of nonmalignant cells results. (a) Three-dimensional confocal images of MDA-MB-468 cells expressing HS-131-positive puncta after a 45 min treatment with 25 μM HS-131. Scale bar, 5 μm. (b) Number of puncta/cell of MDA-MB-468 cells treated with 25 μM HS-131 at increasing time points. (c) HS-131fluorescence and Hsp90 immunoreactivity on the surface of a nonpermeabilized MDA-MB-468 cell. Membrane is labeled green. Scale bar, 5 μm. (d) Number of moving puncta (tracks) detected by LLSM of live cells treated with 10 μM HS-131 or HS-198, or HS-131 competed with 100 μM HS-10. (e) Fluorescence of HS-131 internalization (25 μM, 45 min incubation) after treatment with endocytotic inhibitors. CytoD, cytochalasin D, 2 μM; EIPA, 5-(N-Ethyl-*N*-isopropyl)amiloride, 25 μM; PitStop2, 25 μM; Filipin III, 5.0 μg/mL. (f) Representative Western blot of MCF10A clones showing HER2 and Hsp90 expression. GAPDH was used as an internal loading control. (g) Growth foci in MCF10A cells overexpressing full-length HER2, p110HER2, or p110HER2KD induced with doxycycline. (h) Representative fluorescence images of MCF10A mutants treated with 25 μM HS-131 for 45 min. Scale bar, 50 μm. (i) Quantification of HS-131 fluorescence taken as a ratio of doxycycline-treated cells to noninduced cells. *$p < 0.05$; **$p < 0.001$, univariate ANOVA with Bonferroni's posthoc test. Data are represented as the means ± SEM. See also Figure S3.

avidin-purified lysates, we observed the presence of biotin-labeled Hsp90 in the cell lysates after internalization, suggesting that the external eHsp90 had been biotinylated and actively reinternalized (Figure 2f).

HS-131 Binding Reveals eHsp90 Puncta. Confocal images of HS-131-treated cells revealed striking punctate formations both on the cell surface and within the cell itself, as well as diffuse fluorescence throughout the cell (Figure 3a, Movie S1).

DOI: 10.1021/acschembio.7b00006
ACS Chem. Biol. 2017, 12, 1047−1055

Close examination of the larger structures shows that the average size of these puncta is 0.95 ± 0.04 μm^3 with an average fluorescence intensity of 33.01 ± 10.37 units. Using a standard fluorescence curve (Figure S3f), we estimated the concentration within the puncta of HS-131 to be 4.66 ± 0.05 μM. On the basis of puncta volume and a ratio of 1:1 for HS-131:Hsp90 monomer, we estimate that the larger puncta contain 2659 ± 105 monomers of eHsp90. Accumulation of the puncta intracellularly is time-dependent (Figure 3b).

We demonstrated that formation of the puncta is eHsp90-dependent in multiple ways: First, HS-152, the tethered fluorophore without the ligand, does not form puncta when applied to cells (Figures S3a–c). Second, HS-27, a FITC-tethered Hsp90 inhibitor with a fluorophore moiety structurally unrelated to the Cy5 based fluorophore used in HS-131, forms puncta when applied to tumor cells (Figure S3d). Third, binding of HS-131 and HS-27 to eHsp90 is blocked by structurally distinct Hsp90 inhibitors, such as PUH71 (Figure 2e). Fourth, puncta do not form on nonmalignant cells in the presence of HS-131 or HS-27 (Figure 2a[16]). Additionally, formation of the puncta is reversible within cells. Internal puncta numbers decrease after drug removal, and diffuse fluorescence can be observed throughout the cell (Figure 3a). This diffusion may be a result of exchange with intracellular ATP or the degradation of the internalized eHsp90. Probe aggregates would not be expected to spontaneously dissipate without the addition of an organic solvent.

Live imaging of HS-131-treated cells via confocal and lattice light sheet microscopy (LLSM) reveals active trafficking of puncta (Movie S2), suggesting that their formation is part of an organized biological process. LLSM of live cells was also performed on cells treated with HS-131 alone, HS-198, or HS-131 and HS-10, and spots were tracked over time to investigate any differences in puncta movement and size. HS-131-treated cells exhibited significantly more puncta; however, puncta size and speed of movement did not appear to be affected with various treatments (Figure 3d, Figure S3g,h). HS-131 puncta were competed with HS-10 (Figure 3d). No puncta were observed to travel to or within the nucleus. The puncta are therefore a natural phenomenon occurring in live malignant cells that have been revealed by the HS-131 probe. HS-131 is much smaller than antibodies compared with Hsp90 (Figure S2a); thus, HS-131 is more suited for unobtrusive labeling of eHsp90 puncta. However, colocalization of HS-131 with eHsp90 was confirmed using antibodies (Figure 3c).

Hsp90 is known to undergo conformational changes as it cycles between its ATP- and ADP-bound state, altering its affinity for its clients and cochaperones.[24−26] Biochemical studies using affinity resins to isolate the extracellular pool strongly support this hypothesis; eHsp90 was consistently recovered in highly purified form in the absence of clients, cochaperones, or modifications. Therefore, the probe-bound state may be akin to a locked conformation induced upon drug binding, permanently releasing its clients and cochaperones at the plasma membrane. It is plausible that in this "spent" state, the protein self-aggregates on the membrane to form puncta, and this signals its reinternalization.

eHsp90 Is Actively Internalized. To determine the potential mechanism of eHsp90 reinternalization, we adopted an unbiased approach by investigating the impact of several small molecule inhibitors known to selectively interfere with various mechanisms of protein trafficking in and out of cells. Of the five inhibitors tested, only cytochalasin D (CytoD, actin inhibitor) inhibited HS-131 uptake (Figure 3e), suggesting that eHsp90 internalization is an active endocytotic process reliant upon actin dynamics. Actin polymerization is involved in canonical endocytotic pathways, such as macropinocytosis and clathrin- and caveolin-mediated endocytosis, as well as the flipping of lipid rafts. HS-131 internalization was investigated in cells subjected to a broad screen containing 140 well-characterized siRNAs against known endocytosis-related proteins (Figure S3d and Table S1). Interestingly, none of the tested siRNAs showed a convincing effect on HS-131 internalization. The inability of pharmacological inhibitors or the siRNA screen to definitively highlight any one endocytic pathway may suggest that eHsp90 is internalized through multiple pathways.

Transformation Increases Hsp90 Internalization. In previous reports, expression of eHsp90 correlates with malignant phenotypes in cancer lines.[14,16,27] However, all cancers are derived from the transformation of nonmalignant normally functioning cells. A previous report showed that overexpression of a truncated isoform of HER2 (p110HER2) that lacked the extracellular domain but was still membrane-bound led to enhanced migration, invasion, and xenograft formation of human mammary epithelial cells.[28] MCF10A cells, benign human breast epithelial cells that minimally internalize HS-131, were stably infected with a construct encoding a doxycycline-inducible p110HER2. Upon induction of p110HER2 expression, MCF10A cells exhibited a transformed phenotype as demonstrated by increased growth foci and showed a significant increase in HS-131 internalization (Figures 3f–i). Expression of p110HER2 also increased Hsp90 expression. Whereas overexpression of a kinase-dead version of p110HER2 did increase Hsp90 expression, it did not exhibit a transformed phenotype nor did it promote internalization of HS-131 (Figure 3f,g,i). Thus, p110HER2 may lead to a downstream signaling cascade resulting in a transformed phenotype that can be observed through HS-131 internalization. Triple negative breast tumor cells (e.g., MDA-MB-468 and 4T1) also form puncta and internalize HS-131, suggesting that eHsp90 trafficking is transformation-dependent.

eHsp90 Is Correlated with Tumors *in Vivo*. Our *in vitro* studies suggest that aggressive tumor cell lines, almost exclusively, internalize eHsp90; however, the body is comprised of hundreds of distinct cells with specific functions and in specific microenvironments. The majority of cells are fully differentiated and not actively dividing, whereas some subpopulations of cells are constantly undergoing division and growth, such as the endothelial layer lining the intestinal tract. To determine if nontumor cells express/internalize eHsp90, we performed cryosectioning of mice bearing MDA-MB-468 flank tumors 6 h post HS-131 injection. Probe uptake into the tumor in the live animal was first confirmed in a Licor instrument. Cryosectioning allowed us to observe the biodistribution of fluorescent probes to the histological level throughout the body. Following sacrifice, the animal was cryopreserved and longitudinally cryosectioned in 40-μm slices. Each slice was imaged for fluorescence with an mCherry band filter (excitation 550–590 nm, emission 600–670 nm) as well as bright field (all slice image data can be down loaded at DOI: 10.7924/G8G44N63). The images were reconstructed to create a 3D fluorescence and bright field images of the entire mouse anatomy (Figure 4a and Movie S3). This process allowed for the first time a detailed examination of the complete biodistribution of HS-131 at the histological level in every organ. A control nontreated mouse was also imaged using an EGFP-mCherry dual band filter set. In a parallel study, an MS analysis was conducted on specific fluorescent tissues to confirm the presence of the HS-131 parent ion (m/z = 660.0 $[M+2]^{2+}$; Table S2).

DOI: 10.1021/acschembio.7b00006
ACS Chem. Biol. 2017, 12, 1047−1055

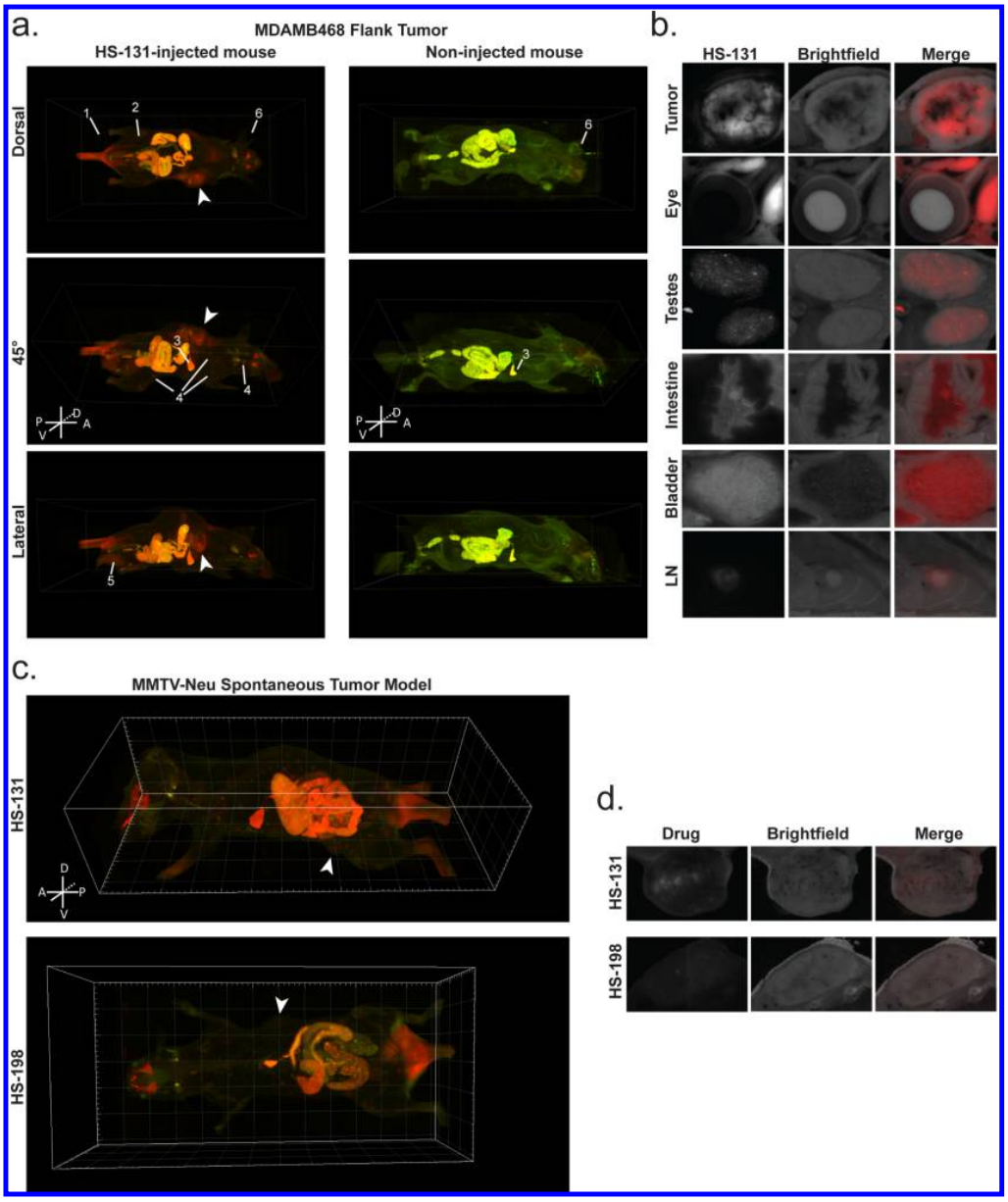

Figure 4. HS-131 visualized in tumors *in vivo*. (a) Left: Mouse with right flank xenograft tumor formed from MDA-MB-468 cells. Right: control mouse (no tumor or drug treatment). Arrowhead, tumor; 1, injection site; 2, bladder; 3, gallbladder; 4, lymph nodes; 5, testes; 6, Harderian glands. (b) Fluorescence and brightfield images in a representative 40-μm section of tumor and other organs; LN, lymph node. (c) Top: HS-131-treated MMTV-neu mouse with spontaneous tumor near left rear leg. Bottom: HS-198-treated MMTV-neu mouse with spontaneous tumor on bottom right abdomen. Arrowheads indicate tumor location. (d) Cross-section of tumor with drug fluorescence. See also Movies S3−S5.

Movie S3 shows a reconstructed flank tumor-bearing HS-131-treated mouse in 3D, first as a bright field image giving gross anatomical reference and then by HS-131 fluorescence. The 3D fluorescence movies and static images in Figure 4a,b show bright fluorescence associated with the gall bladder, bile ducts, and upper intestinal tract in both the injected and noninjected control mouse, suggesting that it may be due to natural fluorescent compounds within the mouse food. Accordingly, MS analysis of the intestines isolated from an animal (6 h postdrug injection) did not show the presence of the parent HS-131 ion (Table S2). In addition, the fluorescence is associated with the digested material in the lumen with no evidence of HS-131 in the gut wall or endothelial lining (Figure 4b). Whereas diarrhea is a dose limiting toxicity associated with many Hsp90 inhibitors in clinical trials and is thought to be related to inhibition of cell proliferation of the endothelial wall lining the upper and lower intestines,[29] the lack of HS-131 uptake suggests that the intestinal endothelium does not internalize eHsp90. Other fluorescent regions include the Harderian glands behind the eye and the retina, the testes, and the lymph nodes (Figure 4a and b). MS analysis of the eyes did not show evidence of the HS-131 parent ion (Table S2). Readily visible nodes include the superficial parotid node in the neck region, the proper axillary node, and the subiliac and sciatic nodes in the forelimb and hindlimb regions, respectively.

DOI: 10.1021/acschembio.7b00006
ACS Chem. Biol. 2017, 12, 1047−1055

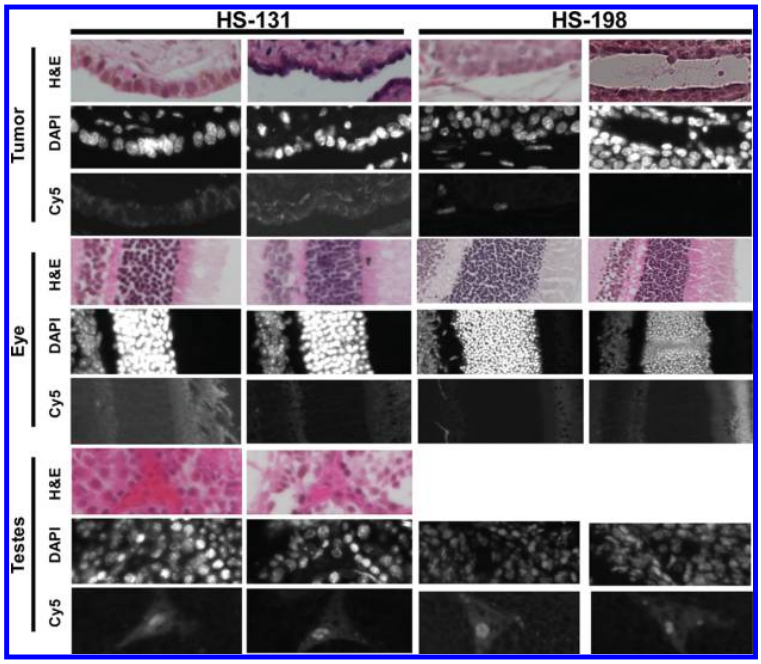

Figure 5. Histology of fluorescent tissues reveals tumor specificity. Serial sections of various organs were imaged, either with H&E staining or with DAPI/Cy5 (drug) fluorescence. Specific drug fluorescence is observed in duct epithelium of tumor cells in the HS-131-treated mouse, but not in the HS-198-treated mouse. Tissues from the HS-198-treated mouse reveal autofluorescence in the rods and cones layer of the eye and in the Leydig cells of the testes.

Higher magnification of the individual lymph nodes shows discrete staining within the node itself confined to a few cellular structures in the hilum. Although Hsp90 inhibition has repressive effects on T lymphocytes,[30] the uptake of HS-131 into the lymph nodes is unlikely to involve T cells because our studies used SCID mice. Other major organs including heart, lungs, liver, kidney, spleen, brain, skeletal muscle, stomach, skin, thyroid, prostate, and fur were completely devoid of HS-131 related fluorescence at the 6 h time point. Aside from fluorescence that had leaked from the injection site, HS-131 was cleared from the entire vasculature by the 6 h time point. No uptake of the HS-131 was detected in the any of the skeletal structures. This was also confirmed by MS analysis (Table S2).

Significant HS-131 fluorescence was detected in the bladder and flank tumor. Overlay of the bright field image section with the fluorescence showed that all of the fluorescence was associated with urine and not the bladder itself (Figure 4b). This was confirmed by MS analysis of the urine that detected the parent ion at a concentration of approximately 50 nM (Table S2). These results suggest HS-131 is primarily eliminated intact through the kidney.

Examination of both the bright field image of the tumor as well as a 3D reconstruction of the tumor mass shows its anatomy including the fibrotic wall, necrotic regions, microvasculature, and live tumor tissue (Figure 4b, Movie S4). HS-131 uptake is exclusively associated with live tumor tissue and not the fibrotic wall or necrotic regions. MS analysis confirmed the presence of the intact parent HS-131 molecule at a concentration of ~325 nM (w.w.; Table S2).

Flank tumors, due to their homogeneity, do not accurately reflect the physiology of human tumors. To investigate the tumor specificity and eHsp90 internalization in a more relevant model of human breast cancer, we turned to the MMTV-neu spontaneous mammary tumor mouse model (Figures 4c,d). Two MMTV-neu mice bearing equal sized mammary tumors (~150 mm^3) were injected in parallel (i.v.) with 25 nmol of HS-131 or the inactive analog HS-198, and after 6 h the animals were cryopreserved and cryosectioned as previously described. Figure 4c and d show that the HS-131 uptake is confined to the tumor in comparison to HS-198, confirming that probe uptake is eHsp90-dependent. Importantly, HS-131 shows the same biodistribution as observed with the flank tumor animal shown in Figure 4a. Movie S5 shows a 3D reconstruction from the HS-131-containing MMTV-neu tumor from Figure 4d compared with that of the HS-198-treated mouse. Interestingly, compared with Movie S4, HS-131 uptake in the MMTV tumor mass is more discrete than the more homogeneous uptake in the flank tumor. Closer inspection *via* histology revealed that HS-131 fluorescence within the MMTV tumor is confined to select areas of ductal epithelial cells (Figure 5). On the basis of studies with isolated breast cell lines, these findings suggest that the cells discretely stained within HS-131 exhibit a malignant phenotype and may be analogous to ductal carcinoma *in situ* (DCIS) in human breast cancer. No uptake was observed in these cells within the tumor isolated from the HS-198-treated animal, again supporting the hypothesis that HS-131 is eHsp90 dependent. In addition, comparison with tissues from the HS-198-treated mice revealed that the previously observed fluorescence within the rod and cone layer of the eyes and the Leydig cells of the testes were due to autofluorescence (Figure 5), consistent with previous reports.[31]

In summary, our imaging studies with HS-131 revealed at the molecular and cellular level that expression and internalization of eHsp90 is a unique phenomenon associated with highly transformed tumor cells. Studies with HS-131 in other tumor cells (e.g., lung cancer and melanoma lines) suggest that expression of eHsp90 is common to cells with an aggressive malignant cellular phenotype (Figure S3i). Our studies highlight

DOI: 10.1021/acschembio.7b00006
ACS Chem. Biol. 2017, 12, 1047−1055

the therapeutic relevance of selectively targeting eHsp90 internalization. First, eHsp90 provides a noninvasive biomarker of malignant behavior. Second, the ability of eHsp90 to be reinternalized with a bound probe clearly indicates the protein can be further exploited as a means of tumor-specific drug delivery. One of the most remarkable results from our studies was the finding that expression of eHsp90 is a rare cellular event in the body and does not occur in normal fully differentiated tissues. Given the rareness of eHsp90 expression on cells, in principle drugs targeting eHsp90 will have a significantly greater therapeutic window than all existing Hsp90 inhibitors and offer a curative outcome rather than conventional therapeutic approach.

METHODS

Cell Culture and Reagents. MDA-MB-468 cells were maintained in DMEM containing 10% (v/v) FBS and penicillin/streptomycin. MCF10A cells were maintained in Brugge's modified medium. Doxycycline was used at a final concentration of 1 μg/mL. Cells were kept in a humidified atmosphere at 37 °C and with 5% CO_2. All cells were acquired from the Duke Cancer Institute Cell Culture Facility. PUH71 was purchased from APExBIO. All chemicals and other reagents were of analytical grade.

HS-131 Internalization Assay and Imaging. Cells were plated on uncoated coverslips in 12 well plates at 150 000 cells/well and were allowed to adhere overnight. HS-131 was diluted in serum-free/phenol red-free DMEM. After drug incubation, the cells were washed with ice-cold PBS, fixed with 1% (w/v) PFA for 10 min, and stained with 5 μg/mL wheat germ agglutinin-488 (WGA-488, Invitrogen) and either Hoescht or DAPI. The coverslips were mounted onto microscope slides using FluorSave (Millipore). Slides were imaged on a Leica SP5 confocal microscope.

Images were analyzed for fluorescence and puncta using ImageJ software using a nonbiased, high-throughput macro. High resolution confocal stacks were deconvolved with Hyugen's Deconvolution Software or AiryScan.

Hsp90 Colocalization. Cells were treated with HS-131 for 30 min on ice. The cells were washed and fixed as above, blocked with 5% (v/v) normal goat serum, and incubated with anti-Hsp90 antibody (sc-7947, Santa Cruz Biotechnology, Inc.), which recognizes both the Hsp90α and Hsp90β isoforms. The coverslips were washed and incubated with secondary antibody conjugated to AlexaFluor-555, washed, and prepared for imaging.

Biotin Internalization Assay. MDA-MB-468 cells were plated 1.0×10^6 cells/well in a six-well plate. Biotin internalization assay was performed as previously described.[23] Lysates were collected as previously described and purified on avidin beads to collect the biotinylated proteins. The biotinylated protein fractions were subjected to Western blot analysis.

MCF10A Transformation. Human HER2 cDNAs for the full-length p185 kDa protein and its p110 kDa fragment were cloned by PCR of cDNA from the T74D cell line. PCR-based site specific mutation was performed to create a p110-kDa kinase inactivation by the K736R mutation. All constructs were confirmed by sequencing. Constructs were cloned into the doxycycline-inducible expression lentivirus plasmids using a modification of a previously described method.[32] For the growth foci assay, cells were trypsinized, and 1000 cells with an inducible construct were plated with 100 000 cells uninfected with MCF10A per well in a six-well plate. Media were replaced every 3–4 days. After 3 weeks, the cells were washed, fixed with ice cold methanol, rinsed, and stained with a 0.4% (v/v) methylene blue solution.

Western Blot Analysis. Lysates were subjected to SDS-PAGE and were subsequently transferred to a PVDF membrane. The membrane was blocked with 5% (w/v) nonfat dry milk in PBS-T (PBS with 0.1% (v/v) Tween); incubated with anti-Hsp90, anti-HER2 (29D8, Cell Signaling Technology), or anti-GAPDH (D16H11, Cell Signaling Technology); washed in PBS-T; incubated with secondary antibody conjugated with HRP; and washed again in PBS-T. The membrane was developed using Clarity Western ECL Blotting Substrate (Bio-Rad) and exposure to film.

Three-Dimensional Mouse Reconstruction. All protocols involving the use of mice were approved by the Duke University IACUC. A wild-type 3-month-old male SCID mouse with a right flank xenograft with MDA-MB-468 cells was injected with 25 nmol HS-131 through the tail vein. Six hours later, the mouse was euthanized, prepared according to the instructions from BioInVision, Inc., and shipped for Cryo-Imaging and reconstruction. An EGFP/mCherry dual band filter set was used for imaging (Chroma Technology Corporation).

Histology. MMTV-neu mice treated with 10 nmol of HS-131 or HS-198 were euthanized, and tumors, eyes, and testes were fixed in neutral-buffered formalin before dehydration and embedding in paraffin blocks. Slices (5-μm-thick) were deparaffinized and either H&E stained or rehydrated and stained with DAPI before mounting. Slides were imaged at 20× magnification on a Zeiss Axio Imager widefield fluorescence microscope equipped with a color camera.

Statistical Analysis. All imaging experiments were performed in duplicate and repeated three times. After testing for normalcy, multivariate analysis of variance (ANOVA) was used to detect significant differences between experiments with more than one factor, and univariate ANOVA was used to detect significant differences between experiments with only one factor. ANOVA results were subjected to Bonferroni posthoc tests to account for differences in sample size. A p value of <0.05 was considered significant. All statistical analysis was performed using IBM SPSS Statistics for Windows, version 20.0. Data are represented as the means ± SEM.

ASSOCIATED CONTENT

Supporting Information

The Supporting Information is available free of charge on the ACS Publications website at DOI: 10.1021/acschembio.7b00006.

Figures S1–S3, Table S1, Table S2, and supplementary methods (PDF)
Movie S1 (AVI)
Movie S2 (AVI)
Movie S3 (AVI)
Movie S4 (AVI)
Movie S5 (AVI)

AUTHOR INFORMATION

Corresponding Author

*Tel.: (919) 613-8606. E-mail: timothy.haystead@dm.duke.edu.

ORCID

Philip F. Hughes: 0000-0002-2217-455X

Author Contributions

▽These authors contributed equally to this work.

Notes

The authors declare the following competing financial interest(s): An international patent-pending application (No. PCT/US2013/031614) exists for several of the small-molecule inhibitors listed in this work.

ACKNOWLEDGMENTS

This work was supported by a grant from the Department of Defense (No. W81XWH-15-1-0072), a Transformative Vision Award (No. W81XWH-12-01-0447) from the Department of Defense, and a National Science Foundation Graduate Research Fellowship (No. DGF1106401). Imaging data used in this publication were produced in collaboration with the Advanced Imaging Center, a facility jointly supported by the Gordon and Betty Moore Foundation and HHMI at HHMI's Janelia Research Campus. Lung cancer, melanoma, and adenocarcinoma

DOI: 10.1021/acschembio.7b00006
ACS Chem. Biol. 2017, 12, 1047–1055

cell lines were a gift from C. Counter at Duke University. Reagents are available upon request.

REFERENCES

(1) Moulick, K., Ahn, J. H., Zong, H., Rodina, A., Cerchietti, L., Gomes DaGama, E. M., Caldas-Lopes, E., Beebe, K., Perna, F., Hatzi, K., Vu, L. P., Zhao, X., Zatorska, D., Taldone, T., Smith-Jones, P., Alpaugh, M., Gross, S. S., Pillarsetty, N., Ku, T., Lewis, J. S., Larson, S. M., Levine, R., Erdjument-Bromage, H., Guzman, M. L., Nimer, S. D., Melnick, A., Neckers, L., and Chiosis, G. (2011) Affinity-based proteomics reveal cancer-specific networks coordinated by Hsp90. *Nat. Chem. Biol. 7*, 818−826.

(2) Taipale, M., Jarosz, D. F., and Lindquist, S. (2010) HSP90 at the hub of protein homeostasis: emerging mechanistic insights. *Nat. Rev. Mol. Cell Biol. 11*, 515−528.

(3) Whitesell, L., and Lindquist, S. L. (2005) HSP90 and the chaperoning of cancer. *Nat. Rev. Cancer 5*, 761−772.

(4) Neckers, L., and Workman, P. (2012) Hsp90 molecular chaperone inhibitors: are we there yet? *Clin. Cancer Res. 18*, 64−76.

(5) Pearl, L. H., and Prodromou, C. (2006) Structure and mechanism of the Hsp90 molecular chaperone machinery. *Annu. Rev. Biochem. 75*, 271−294.

(6) Trepel, J., Mollapour, M., Giaccone, G., and Neckers, L. (2010) Targeting the dynamic HSP90 complex in cancer. *Nat. Rev. Cancer 10*, 537−549.

(7) Jhaveri, K., Taldone, T., Modi, S., and Chiosis, G. (2012) Advances in the clinical development of heat shock protein 90 (Hsp90) inhibitors in cancers. *Biochim. Biophys. Acta, Mol. Cell Res. 1823*, 742−755.

(8) Pillarsetty, N. C.-L. E., Punzalan, B., Santos, E., Kang, Y., Taldone, T., Zatorska, D., Chiosis, G., Lewis, J., and Larson, S. (2010) Radioiodination, biodistribution, and PET imaging studies of Hsp90 inhibitor [^{124}I]-PU-H71. *J. Nucl. Med. 51*, 556.

(9) Taldone, T., Zatorska, D., Ochiana, S. O., Smith-Jones, P., Koziorowski, J., Dunphy, M. P., Zanzonico, P., Bolaender, A., Lewis, J. S., Larson, S. M., Chiosis, G., and Pillarsetty, N. V. (2016) Radiosynthesis of the iodine-124 labeled Hsp90 inhibitor PU-H71. *J. Labelled Compd. Radiopharm. 59*, 129−132.

(10) Kamal, A., Thao, L., Sensintaffar, J., Zhang, L., Boehm, M. F., Fritz, L. C., and Burrows, F. J. (2003) A high-affinity conformation of Hsp90 confers tumour selectivity on Hsp90 inhibitors. *Nature 425*, 407−410.

(11) Woodford, M. R., Truman, A. W., Dunn, D. M., Jensen, S. M., Cotran, R., Bullard, R., Abouelleil, M., Beebe, K., Wolfgeher, D., Wierzbicki, S., Post, D. E., Caza, T., Tsutsumi, S., Panaretou, B., Kron, S. J., Trepel, J. B., Landas, S., Prodromou, C., Shapiro, O., Stetler-Stevenson, W. G., Bourboulia, D., Neckers, L., Bratslavsky, G., and Mollapour, M. (2016) Mps1Mediated Phosphorylation of Hsp90 Confers Renal Cell Carcinoma Sensitivity and Selectivity to Hsp90 Inhibitors. *Cell Rep. 14*, 872−884.

(12) Murshid, A., Gong, J., and Calderwood, S. K. (2014) Hsp90-peptide complexes stimulate antigen presentation through the class II pathway after binding scavenger receptor SREC-I. *Immunobiology 219*, 924−931.

(13) McCready, J., Wong, D. S., Burlison, J. A., Ying, W., and Jay, D. G. (2014) An Impermeant Ganetespib Analog Inhibits Extracellular Hsp90-Mediated Cancer Cell Migration that Involves Lysyl Oxidase 2-like Protein. *Cancers 6*, 1031−1046.

(14) Becker, B., Multhoff, G., Farkas, B., Wild, P. J., Landthaler, M., Stolz, W., and Vogt, T. (2004) Induction of Hsp90 protein expression in malignant melanomas and melanoma metastases. *Exp. Dermatol. 13*, 27−32.

(15) Sidera, K., and Patsavoudi, E. (2008) Extracellular HSP90: conquering the cell surface. *Cell Cycle 7*, 1564−1568.

(16) Barrott, J. J., Hughes, P. F., Osada, T., Yang, X. Y., Hartman, Z. C., Loiselle, D. R., Spector, N. L., Neckers, L., Rajaram, N., Hu, F., Ramanujam, N., Vaidyanathan, G., Zalutsky, M. R., Lyerly, H. K., and Haystead, T. A. (2013) Optical and radioiodinated tethered Hsp90 inhibitors reveal selective internalization of ectopic Hsp90 in malignant breast tumor cells. *Chem. Biol. 20*, 1187−1197.

(17) Imai, T., Kato, Y., Kajiwara, C., Mizukami, S., Ishige, I., Ichiyanagi, T., Hikida, M., Wang, J. Y., and Udono, H. (2011) Heat shock protein 90 (HSP90) contributes to cytosolic translocation of extracellular antigen for cross-presentation by dendritic cells. *Proc. Natl. Acad. Sci. U. S. A. 108*, 16363−16368.

(18) Fadden, P., Huang, K. H., Veal, J. M., Steed, P. M., Barabasz, A. F., Foley, B., Hu, M., Partridge, J. M., Rice, J., Scott, A., Dubois, L. G., Freed, T. A., Silinski, M. A., Barta, T. E., Hughes, P. F., Ommen, A., Ma, W., Smith, E. D., Spangenberg, A. W., Eaves, J., Hanson, G. J., Hinkley, L., Jenks, M., Lewis, M., Otto, J., Pronk, G. J., Verleysen, K., Haystead, T. A., and Hall, S. E. (2010) Application of chemoproteomics to drug discovery: identification of a clinical candidate targeting hsp90. *Chem. Biol. 17*, 686−694.

(19) Hughes, P. F., Barrott, J. J., Carlson, D. A., Loiselle, D. R., Speer, B. L., Bodoor, K., Rund, L. A., and Haystead, T. A. (2012) A highly selective Hsp90 affinity chromatography resin with a cleavable linker. *Bioorg. Med. Chem. 20*, 3298−3305.

(20) Lee, H., Mason, J. C., and Achilefu, S. (2006) Heptamethine cyanine dyes with a robust C-C bond at the central position of the chromophore. *J. Org. Chem. 71*, 7862−7865.

(21) Wycisk, V., Pauli, J., Welker, P., Justies, A., Resch-Genger, U., Haag, R., and Licha, K. (2015) Glycerol-based contrast agents: a novel series of dendronized pentamethine dyes. *Bioconjugate Chem. 26*, 773−781.

(22) Lu, X., Bennet, B., Mu, E., Rabinowitz, J., and Kang, Y. (2010) Metabolomic changes accompanying transformation and acquisition of metastatic potential in a syngeneic mouse mammary tumor model. *J. Biol. Chem. 285*, 9317−9321.

(23) Gabriel, L., Stevens, Z., and Melikian, H. (2009) Measuring plasma membrane protein endocytic rates by reversible biotinylation. *J. Visualized Exp.*, DOI: 10.3791/1669.

(24) Prodromou, C., Roe, S. M., O'Brien, R., Ladbury, J. E., Piper, P. W., and Pearl, L. H. (1997) Identification and structural characterization of the ATP/ADP-binding site in the Hsp90 molecular chaperone. *Cell 90*, 65−75.

(25) Obermann, W. M., Sondermann, H., Russo, A. A., Pavletich, N. P., and Hartl, F. U. (1998) In vivo function of Hsp90 is dependent on ATP binding and ATP hydrolysis. *J. Cell Biol. 143*, 901−910.

(26) Scheibel, T., Neuhofen, S., Weikl, T., Mayr, C., Reinstein, J., Vogel, P. D., and Buchner, J. (1997) ATP-binding properties of human Hsp90. *J. Biol. Chem. 272*, 18608−18613.

(27) Eustace, B. K., Sakurai, T., Stewart, J. K., Yimlamai, D., Unger, C., Zehetmeier, C., Lain, B., Torella, C., Henning, S. W., Beste, G., Scroggins, B. T., Neckers, L., Ilag, L. L., and Jay, D. G. (2004) Functional proteomic screens reveal an essential extracellular role for hsp90 alpha in cancer cell invasiveness. *Nat. Cell Biol. 6*, 507−514.

(28) Ward, T. M., Iorns, E., Liu, X., Hoe, N., Kim, P., Singh, S., Dean, S., Jegg, A. M., Gallas, M., Rodriguez, C., Lippman, M., Landgraf, R., and Pegram, M. D. (2013) Truncated p110 ERBB2 induces mammary epithelial cell migration, invasion and orthotopic xenograft formation, and is associated with loss of phosphorylated STAT5. *Oncogene 32*, 2463−2474.

(29) Goldman, J. W., Raju, R. N., Gordon, G. A., El-Hariry, I., Teofilivici, F., Vukovic, V. M., Bradley, R., Karol, M. D., Chen, Y., Guo, W., Inoue, T., and Rosen, L. S. (2013) A first in human, safety, pharmacokinetics, and clinical activity phase I study of once weekly administration of the Hsp90 inhibitor ganetespib (STA-9090) in patients with solid malignancies. *BMC Cancer 13*, 152.

(30) Bae, J., Munshi, A., Li, C., Samur, M., Prabhala, R., Mitsiades, C., Anderson, K. C., and Munshi, N. C. (2013) Heat shock protein 90 is critical for regulation of phenotype and functional activity of human T lymphocytes and NK cells. *J. Immunol. 190*, 1360−1371.

(31) Yang, Y., and Honaramooz, A. (2012) Characterization and quenching of autofluorescence in piglet testis tissue and cells. *Anat Res. Int. 2012*, 820120.

(32) Shin, K. J., Wall, E. A., Zavzavadjian, J. R., Santat, L. A., Liu, J., Hwang, J. I., Rebres, R., Roach, T., Seaman, W., Simon, M. I., and Fraser, I. D. (2006) A single lentiviral vector platform for microRNA-based conditional RNA interference and coordinated transgene expression. *Proc. Natl. Acad. Sci. U. S. A. 103*, 13759−13764.

DOI: 10.1021/acschembio.7b00006
ACS Chem. Biol. 2017, 12, 1047−1055